Wind Energy

WIND ENERGY
Wind Energ. (2016)
Published online in Wiley Online Library (wileyonlinelibrary.com). DOI: 10.1002/we.2018

RESEARCH ARTICLE

Aero-structural design optimization of vertical axis wind turbines

Gabriele Bedon and Ernesto Benini
Università degli Studi di Padova, Dipartimento di Ingegneria Industriale, Via Venezia 1, 35131 Padova, Italy

ABSTRACT

In the last decade, vertical axis wind turbines acquired notable interest in the renewable energy field. Different techniques are available to perform aerodynamic and structural simulation of these complex machines, but, to the authors' best knowledge, a comprehensive approach, which includes an automatic optimization algorithm, has never been developed. In this work, a methodology to conduct an efficient aero-structural design of Darrieus vertical axis wind turbine is presented. This relies on a code-to-measurement validated simulation tool based on Blade Element-Momentum algorithm adopting a particular set of aerodynamic coefficients, and a code-to-code validated structural model based on the Euler–Bernoulli beam theory. The algorithms are coupled with a Genetic Algorithm to perform the optimization. The adopted decisional parameters allow to completely vary the blade shape and the airfoil geometry to reduce the structural stress and improve the aerodynamic performance. Different individuals are explored to perform a wide aerodynamic and structural analysis of improved configurations. Copyright © 2016 John Wiley & Sons, Ltd.

KEYWORDS
vertical axis wind turbine; aero-structural optimization; genetic algorithm; bem model; structural simulation

Correspondence
G. Bedon, Università degli Studi di Padova, Dipartimento di Ingegneria Industriale, Via Venezia 1, 35131 Padova, Italy.
E-mail: gabriele.bedon@dii.unipd.it

Received 20 October 2015; Revised 12 March 2016; Accepted 15 July 2016

NOMENCLATURE

a [−]	Induction factor
A [m^2]	Rotor swept area
ch [m]	Airfoil chord
C_P [−]	Rotor power coefficient
$C_{P,max}$ [−]	Maximum rotor power coefficient in the range
h [%]	Percentage of the rotor height
n_{bad} [−]	Total number of sectors for which the Aerodynamic Model does not converge
v [m/s]	Free-stream wind velocity
v_{blade} [m/s]	Velocity at the upwind or downwind blade
λ [−]	Tip speed ratio
σ_z [MPa]	Flatwise stress
$\sigma_{z,max}$ [MPa]	Maximum flatwise stress
$\sigma_{z,mean}$ [MPa]	Mean flatwise stress
$\sigma_{z,min}$ [MPa]	Minimum flatwise stress

1. INTRODUCTION

Academic and industrial interest towards vertical axis wind turbines (VAWTs) is recently experiencing a renovated growth after the initial numerical and experimental activities performed in the 1980s.[1] Different turbine architectures are nowadays being investigated with the aim of decreasing the cost of energy and obtaining high reliability. Similarly to the horizontal axis design, research on VAWTs is primarily focused on rotors with considerable diameter size for offshore installations. Among the most notably recent projects, FP7 Deepwind[2] and FP7 Inflow[3] are devoted to prove technology for very large, multi-megawatt, offshore installations.

The technology related to blade construction and materials experienced several improvements from forerunner prototypes, e.g., pultrusion of fiber-composite materials[4] in lieu of extruded aluminum.[5] The same level of improvement can not however be asserted for the aerodynamic design analysis. Computational fluid dynamics techniques for iterative solution of the unsteady Reynolds-averaged Navier–Stokes equations provide strongly reliable results on the aerodynamic loads. However, they lack of the necessary alacrity for the design process because of the considerable computational time required to perform complete estimations.[6]

The aerodynamic design of VAWTs is therefore still performed using semi-empirical models based on the Blade Element-Momentum (BEM) theory,[7–9] vortex theory[10,11] and actuator cylinder models.[12] These models are fast to compute a reliable prediction for the rotor aerodynamic performance, but their application is limited mainly to low solidity rotors.[13] These models have been continuously adopted and improved over the years, by providing correction models[14] and performing validations.[15,16]

On the other hand, the structural analysis of VAWTs is generally conducted by adopting a finite element analysis (FEA) and provides reliable results, considering both steady[5,17] and unsteady approaches.[18,19] This peculiar flexibility is driven by the fact that, differently from the horizontal design,[20] in VAWTs, centrifugal forces are the mainly contribution to the rotor load system.[21,22]

BEM and FEA can be efficiently coupled to perform a complete aero-structural analysis of the rotor. Given the considerable rotor size for offshore applications, a particular attention is given to structural aspects, which led to adopt in several prototypes a shape similar to the Troposkien.[23] The Troposkien is the particular shape assumed by a rotating rope at zero gravity, whose main characteristic is the minimization of bending stresses.[24] While this simplification does not lead to important collateral stresses for small size rotors, this is not the case when big offshore rotors are considered. Variations from the Troposkien were proposed by several authors,[25,26] whereas Roscher *et al.*[27] provided the blade shape and structural design to minimize the mass to rotor area ratio. A complete optimization considering both aerodynamic performance and loads is not, however, documented in the open literature.

In this work, a new methodology to provide the optimal blade shape and chord distribution for a VAWT rotor is presented. This methodology involves the combined use of a validated aero-structural code, to provide reliable structural and aerodynamic analyses, coupled with an advanced optimization tool based on a genetic algorithm, to perform a wide and efficient exploration of the non-smooth solution space.[28] A baseline rotor is selected to perform the optimization and provide the optimal blade shape and chord distribution to maximize the power coefficient and minimize the flatwise stress.

2. METHODS

A baseline configuration is selected to perform algorithm validation and proceed with design optimization. The selected baseline is the widely documented Sandia 34 m wind turbine,[5,17,25] whose main characteristics are presented in Section 2.1. The aerodynamic and structural models adopted in the present work and their validation are presented in Section 2.2 and 2.3. The optimization algorithm, presented in Section 2.4, is coupled with the simulation codes, providing an equilibrium solution in every blade azimuthal position, as presented in Section 2.5.

2.1. Baseline

The rotor architecture of Sandia 34 m rotor is considered as baseline. The rotor shape is varied from the original Troposkien shape to account for gravity effects, and the blade airfoil is changed along the span for both structural and aerodynamic considerations. The blade characteristics and shape are reported in Table I and shown in Figure 1.

Several experimental results are reported in the reference papers. In particular, aerodynamic performance in terms of power production and power coefficients are provided for different wind speeds at three fixed rotational speeds: 28 rpm, 34 rpm and 38 rpm.[25] Moreover, operational flatwise stress linked to gravitational and centrifugal loads are provided for two rotational speeds:[17] 28 rpm and 40 rpm. Model validations are conducted by comparison with such data.

Table I. Main characteristics of the Sandia 34 m turbine.

Height [m]	41.9
Equatorial radius [m]	17.1
Number of blades [-]	2
Rated rotational speed [rpm]	37.5
Rated power [kW]	500
Rated wind speed [m s^{-1}]	12.5
Cut-out wind speed [m s^{-1}]	20

DOI: 10.1002/we

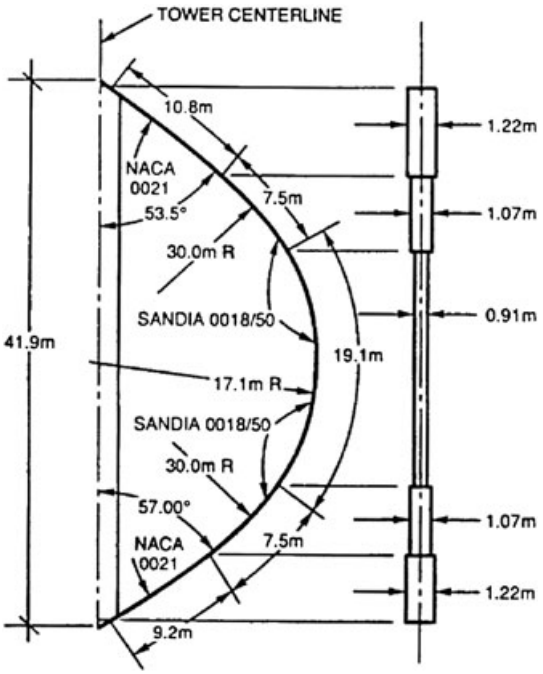

Figure 1. Sandia 34 m: rotor shape, along with chord and thickness distributions.[25]

2.2. Aerodynamic model

The aerodynamic model adopted in the present work is the double multiple streamtube BEM model, originally developed by Glauert[29] and further developed for VAWT simulation by Strickland[7] and Paraschivoiu.[8,9]

The model is widely adopted in literature and a complete code-to-measurement validation, which includes the baseline, is reported by Bedon *et al.*.[30] The aerodynamic database adopted is provided by Jacobs[31] for the NACA 0021 airfoil and by Gregorek[32] for the SAND 0018/50 profile. Database availability for SAND 0018/50 is limited to high Reynolds numbers ($1.410 \cdot 10^6$ and $2.520 \cdot 10^6$), which is however, compatible with the rotor operative conditions. The simulation is performed with a mesh of 160 vertical and 40 azimuthal divisions. The aerodynamic performance estimated with the aerodynamic model compared with the experimental results for the baseline rotor[25] are reported in Figure 2.

At rotational speeds of 28 rpm and 34 rpm, the numerical model over-predicts the experimental power curve. The shift is however characterized by a constant value in the whole operative range and does not affect the position of the peak efficiency. At 38 rpm, a good agreement is registered for tip speed ratios λ higher than 8. At lower values, the experimental curve presents a steep decrease linked to the activation of the aerodynamic brake, which is not simulated by the aerodynamic model.

The aerodynamic model overall provides accurate performance estimations with respect to the experimental results. The required computational time to complete a simulation is very limited, and therefore, the performance model is suitable for optimization purposes.

2.3. Structural model

The FEA model adopted by Sandia involves Euler–Bernoulli beam elements[17] to perform the blade modelization. Each blade section is modeled with a different number of elements, which is shown in Figure 3. Each element matrix is calculated with the particular properties of the blade section or joint, considering the real weight measured from the rotor prototype. The blades' attachments to the central shaft are instead modeled considering two series of two beam elements per blade (the so-called "mini-struts").

As a first step to perform a code-to-experiment validation of the mass and properties calculated for the generic airfoil section, a beam model is created using the commercial software Ansys APDL 14.5 (ANSYS, Inc., Canonsburg, Pennsylvania, USA). Each blade is modeled with a total of 160 elements whereas each mini-strut with one element, BEAM189 3-D Quadratic Finite Strain Beam.[33] The comparison between the experimental data, the numerical predictions provided by Sandia Model and Ansys 14.5 considering the gravitational load and the inertial load for two rotational speeds, are reported

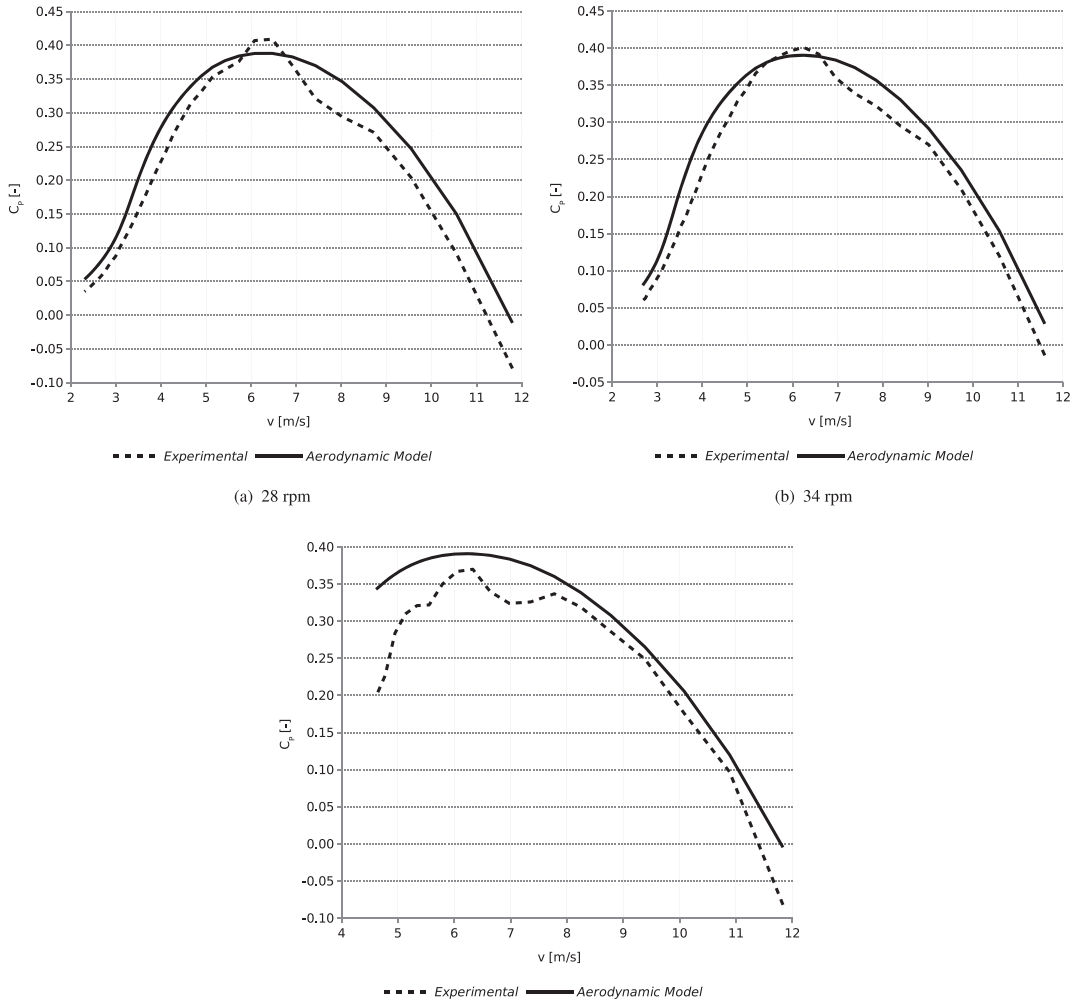

Figure 2. Aerodynamic performance estimated with the aerodynamic model compared with the experimental results for the baseline rotor.[30]

in Figure 4. A good agreement between the numerical predictions provided by Sandia and Ansys 14.5 is registered over the whole blade range, showing a similar accuracy with respect to the experimental data. A slight difference in the stress peak is, nevertheless, registered when the rotational speed is 28 rpm. On the other hand, the Sandia model adopts the real mass and property for every blade section, which are referred to be measured from the full scale rotor but are not provided in the reference paper; differences from the theoretical values, which can lead to discrepancies in numerical stresses, are therefore expected.

A model based on the 2-D Euler–Bernoulli beam theory[34] is additionally created ("Structural Model"), and its results compared with the validated Ansys 14.5 model. The mini-struts increase the complexity of the simulation and lead to a lack in code reliability during the optimization process because of the difficulty to provide a suitable design for different rotor architectures: these are not implemented in the Structural Model and are therefore removed also from the validated Ansys model. The simulation conducted with the gravitational and inertial loads for two rotational speeds is again performed, and the results are reported in Figure 5. A very good agreement between the Structural Model and Ansys 14.5 predictions is registered for the two rotational speeds, whereas a difference is evidenced in the proximity of the blade segment joints in the gravitational simulation. This particular difference can be again related to peculiar devices introduced in the blade; the joints, which are used to couple different blade segments, are not widely documented in the reference and are modeled as concentrated mass in both numerical models. Moreover, Ansys 14.5 adopts a different beam model compared with the one

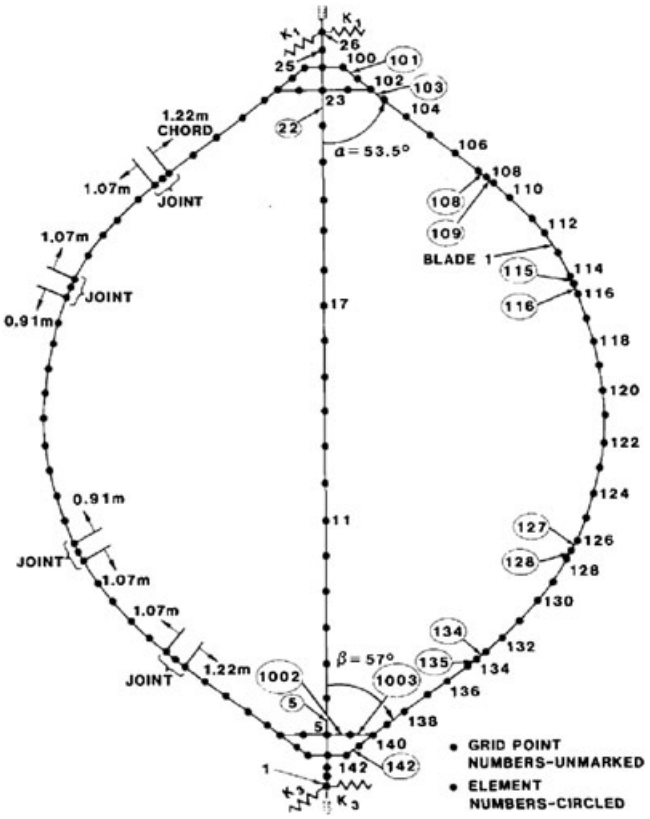

Figure 3. Finite element mesh adopted by Sandia to estimate the stress in the 42m rotor.[17]

adopted in the Structural Model (3-D Timoshenko versus 2-D Euler–Bernoulli), leading to differences in the final flatwise stress. However, since the simulation will be conducted with a spinning rotor and given the very good agreement between the two numerical codes, the Structural Model is considered as code-to-code validated.

2.4. Optimization algorithm

The optimization algorithm is adopted in order to find one or a set of solutions that outperform the baseline design considering different targets. The genetic algorithm is one particular type of heuristic optimization algorithms, created taking into inspiration the Darwinian natural evolution to provide improved solutions.[35]

The adopted multi-objective genetic algorithm is based on the formulation from Deb[28] and is implemented as a tool in the commercial software MATLAB (MathWorks, Natick, Massachusetts, USA).[36] The algorithm is programmed to perform an elitism selection based on the phenotype distance, a roulette wheel parent selection, an intermediate crossover and a mutation function based on the Gaussian distribution. A complete description of these techniques can be found in Goldberg's study.[35] A total of 100 individuals are evaluated and evolved for 200 generations, providing a suitable range for the optimization process. Among the individuals of the first generations, the Sandia baseline is included.

The genetic algorithm provides a total of 20 decision variables ("genes"), which are interpreted by the geometry generator as follows:

- Genes 1 → 10: coordinates of 5 control points of a Bézier curve that describes the blade shape;
- Genes 11 → 15: chord length for the five blade sections;
- Genes 16 → 20: percentage of the rotor height for the five blade segments.

The value of the fitness function denotes the "goodness" of a solution and drives the algorithm in performing the optimization. In the current implementation, it tends to be minimized. In this work, both the aerodynamic performance and the structural stress are object of interest. The baseline design provides the peak power coefficient for tip speed ratios λ between 4 and 8 and this range is considered in the optimization routine. A multi-objective approach is adopted, which

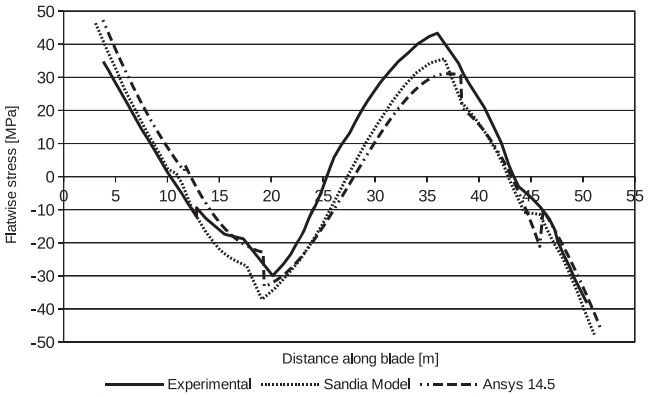

(a) Gravity

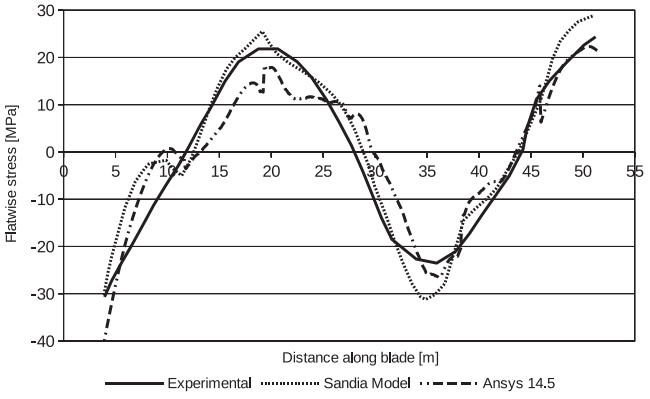

(b) 28 rpm

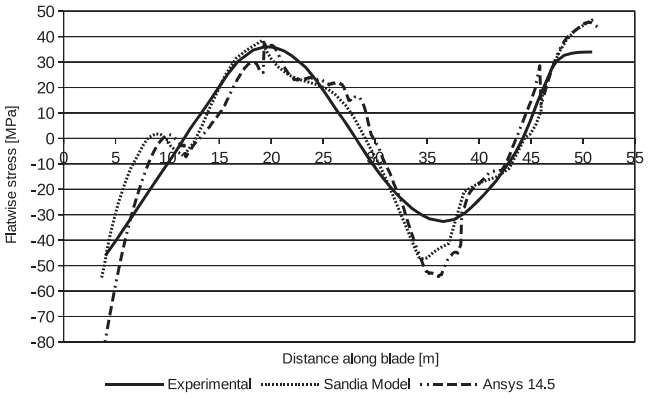

(c) 40 rpm

Figure 4. Comparison between the experimental data, the numerical predictions provided by Sandia and Ansys 14.5 considering the gravitational load and the inertial load for two rotational speeds.

provides a Pareto front with the optimal results (each solution in the front is not dominated, i.e., there is not another solution with both fitness values improved[35]). The optimization procedure aims at the following:

- Maximization of the maximum product between power coefficient and swept area, $C_P \cdot A$. This value provides a reference value for the power production, which is not, however, influenced by the free stream wind speed, being the latter varied in the adopted range.
- Minimization of the maximum flatwise stress σ_z along the blade, considering both the standstill and rotating operative conditions.

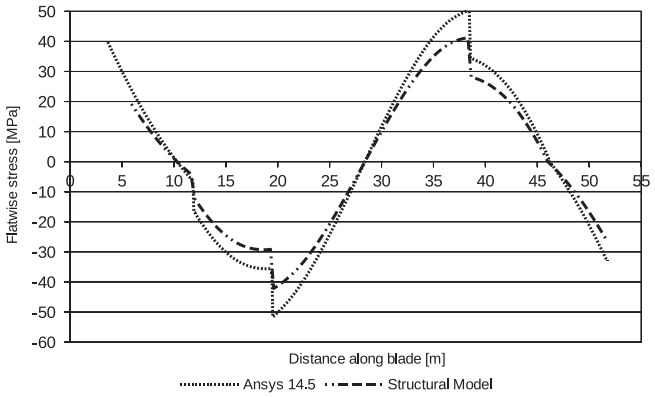

(a) Gravity

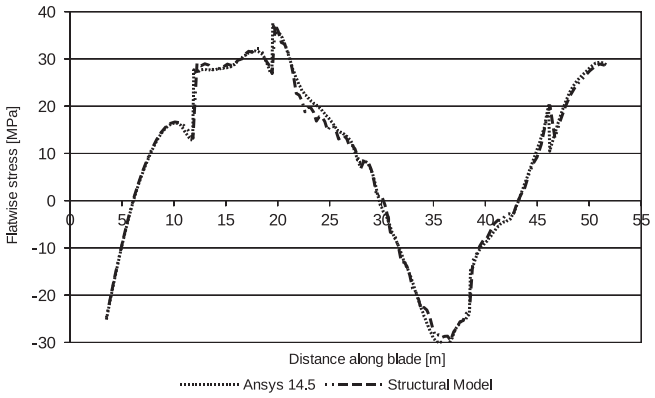

(b) 28 rpm

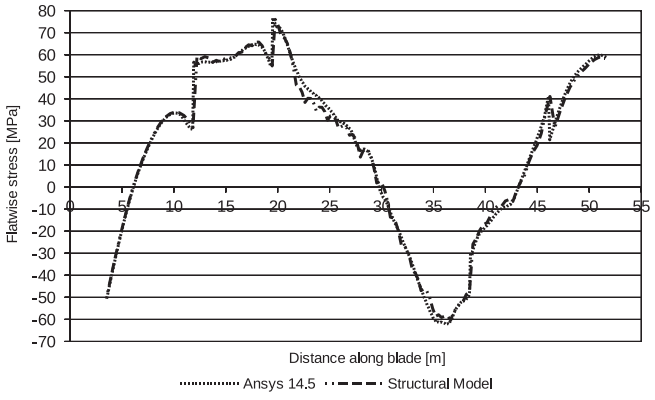

(c) 40 rpm

Figure 5. Comparison between the experimental data and the numerical predictions without "mini-struts" provided by Ansys 14.5 and the Structural Model considering the gravitational load and the inertial load for two rotational speeds.

- The total number of sectors for which the Aerodynamic Model is not converged is considered. This value is included as an additional objective to address the optimization algorithm towards solutions, which are reliably simulated by the Aerodynamic Model, and it will be considered as a filter during the post-processing phase to exclude failed individuals.

The choice of these three objectives allows to obtain turbine optimized configurations characterized by both high efficiency and low flatwise stress. The fitness values are the following:

$$\text{fitness} = [-(C_P)_{\max}; \sigma_z, \max; n_{\text{bad}}] \tag{1}$$

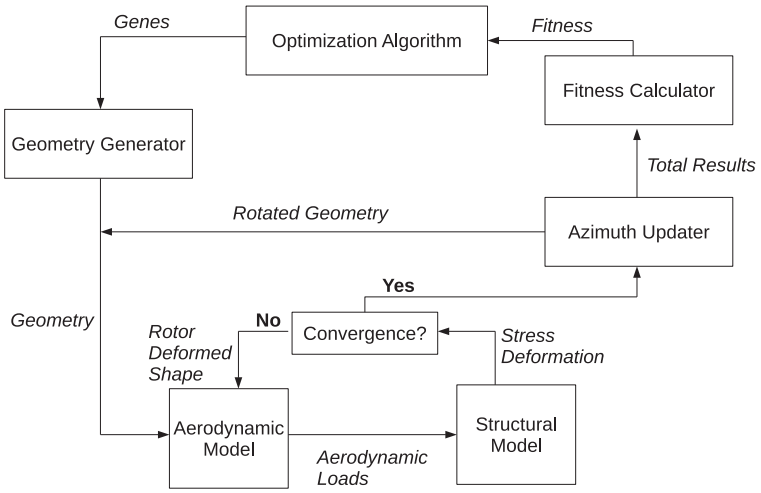

Figure 6. Optimization loop.

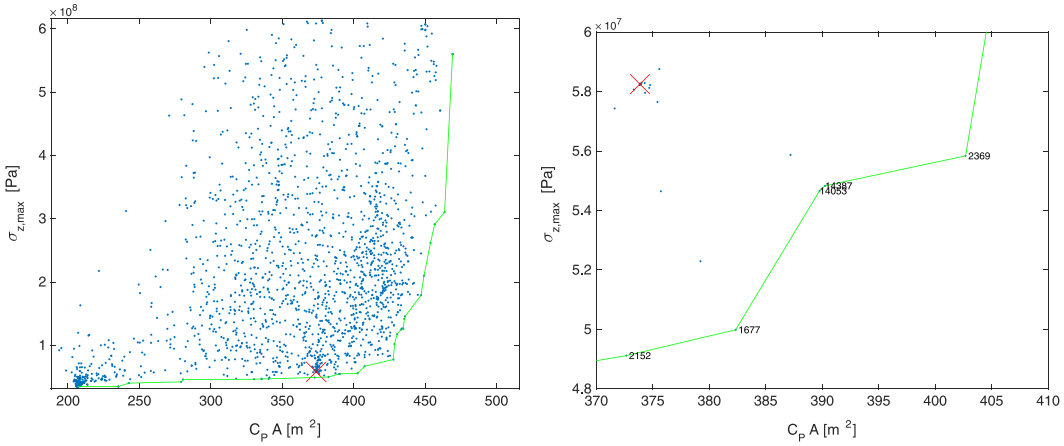

(a) Pareto (b) Localized Pareto

Figure 7. Pareto front and its magnification near the baseline configuration (red cross) for two fitness values and considering a maximum percentage of 1% for the failed simulated sectors.

2.5. Code coupling

The Structural Model, Aerodynamic Model and Optimization Algorithm are coupled to create a loop algorithm as shown in Figure 6.

The geometry generated by the Geometry Generator is first simulated using the Aerodynamic Model, whose results are passed to the Structural Model to estimate the flatwise stress and deformation. The deformed shape is simulated again with the Aerodynamic Model, and the iterative procedure is repeated until convergence in deformation is reached. This sub-loop is evaluated for all the azimuthal positions in the mesh. Finally, the fitness calculator provides the Optimization Algorithm with the fitness vector calculated as previously described.

3. RESULTS AND DISCUSSION

The optimization routine provided a Pareto front of non-dominated solutions. Among the three values in the fitness function, the third objective is considered as a filter to establish the reliability of the simulation; a maximum percentage of 1% for the total failed simulated sectors is accepted. The Pareto front considering the first two fitness values is shown in Figure 7(a). The baseline solution is highlighted with a red cross; a magnification of the Pareto front near the baseline solution is shown in Figure 7(b).

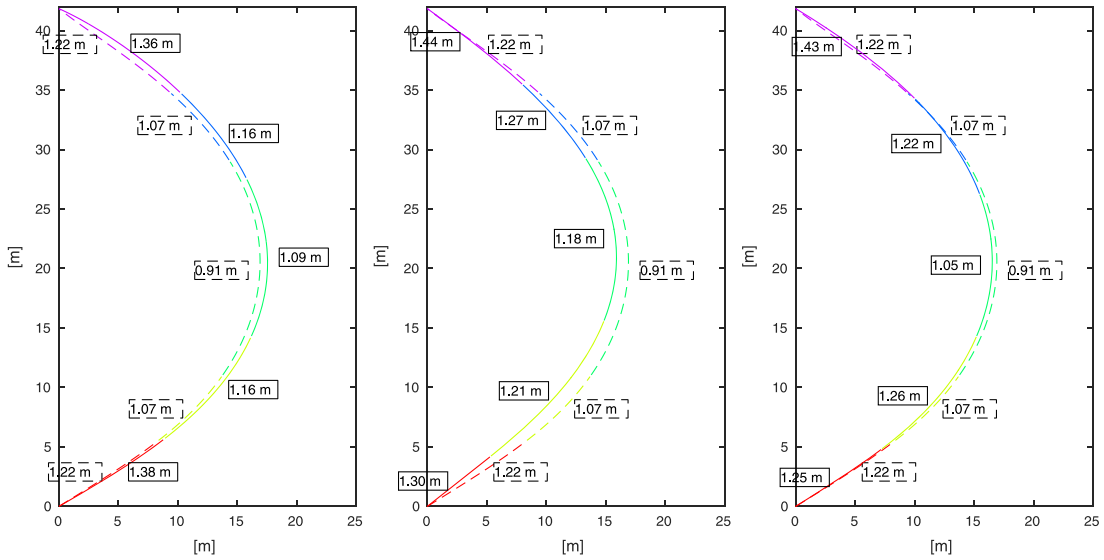

(a) Maximum $C_P A$ (b) Minimum σ_z (c) Trade-off

Figure 8. A selection of three individuals from the Pareto front that dominate the baseline solution are the following: blade shape, segment position and chord lengths for the individual (solid lines and chord values in solid boxes), and baseline (dashed lines and chord values in dashed boxes) solutions. (a) Maximum $C_P A$, (b) Minimum σ_Z and (c) Trade-off.

Table II. Chord lengths and percentage of the rotor height for the five blade segments of the selected individuals.

Baseline		Maximum $C_P A$		Minimum σ_Z		Trade-off	
ch [m]	h [%]	ch [m]	h [%]	ch [m]	h [%]	ch [m]	h [%]
1.22	16.9	1.36	16.9	1.44	15.0	1.43	18.1
1.07	13.8	1.16	17.5	1.27	15.0	1.22	19.4
0.91	43.1	1.09	31.3	1.18	32.5	1.05	28.1
1.07	13.1	1.16	20.6	1.21	27.5	1.26	23.1
1.22	13.1	1.38	13.7	1.30	10.0	1.25	11.3

The individuals that dominate the baseline solution are named in the magnification of the Pareto front in Figure 7(b). Three individuals are of particular interest thanks to their position with respect to the baseline:

- Individual 2152: characterized by a similar value of aerodynamic performance ($C_P A$), but a maximum flatwise stress reduced by 16%;
- Individual 2369: characterized by a similar value of maximum flatwise stress, but aerodynamic performance increased by 8%;
- Individual 14387: selected among the individuals that dominate the baseline solution, it shows an increase of aerodynamic performance of 4%, and a reduction of the maximum flatwise stress of 6%.

These three individuals are characterized by different blade shapes, segments and chord lengths and are shown in Figure 8 (solid lines and chord values in solid boxes) compared against the baseline configuration (dashed lines and chord values in dashed boxes). The chord lengths and the percentage of the rotor height for the five blade segments of the selected individuals are also reported in Table II.

The three solutions need to be discussed specifically from the aerodynamic and structural point of view to highlight the different aspects of the optimization process.

3.1. Aerodynamic analysis

The maximization of the aerodynamic performance value $C_P A$ is obtained, as expected, by a configuration that also provides an increased swept area, see Figure 8(a). Nevertheless, the aerodynamic power coefficients C_P for the three configurations show increased peak values, which are also shifted towards lower values of the tip speed ratios λ, as shown in Figure 9. The peak values and their tip speed ratios for the different configurations are reported in Table III.

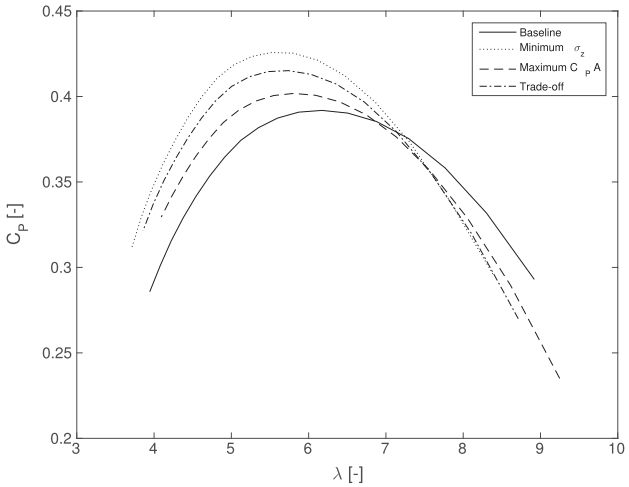

Figure 9. Power coefficient versus tip speed ratio for the baseline and optimized configurations.

Table III. Peak power coefficient and relative tip speed ratio for the baseline and optimized configurations.

Configuration	$C_{P,\max}$	$\lambda\|_{C_{P,\max}}$
Baseline	0.3919	6.1728
Maximum C_PA	0.4018	5.8071
Minimum σ_z	0.4258	5.5211
Trade-off	0.4151	5.7376

The increase of the fitness target C_PA is therefore linked to an increase in both the swept area and the maximum power coefficient. To understand the variation of this second factor, which is the most important for the efficiency of a wind turbine, considerations based on the amount of energy extracted from the airflow can be conducted. The parameter that describes the energy extraction is the "induction factor" a, defined as follows:

$$a = 1 - \frac{v_{\text{blade}}}{v} \tag{2}$$

being v_{blade} the wind velocity, the blade section and v the free-stream wind speed. The induction factor varies between 0 (no absorption) and 1 (complete extraction). The adopted BEM algorithm, without the Glauert correction[29] for high induction factors, is considered reliable only for values lower than 0.5. The contour plots of the upwind induction factors for the baseline and optimized configurations operating at the maximum power coefficient conditions are reported in Figure 10. The observed discontinuities are linked to the different airfoil geometries (type and chord) that are placed next each other along the blade length, whose different characteristics vary the energy extraction.

The induction factors of the baseline configuration (Figure 10(a)) are lower than those of the maximum C_PA configuration (Figure 10(b)). The values are increased in the central segments of the rotor, where the radius and the aerodynamic torque are higher. In these sections, the chord values are increased by 8% and 19%; the optimization algorithm leads the result towards a higher solidity, which increases the interaction with the air to an optimal value without penalizing the flatwise stress.

The configuration with the minimum flatwise stress σ_z is characterized by a reduced swept area (Figure 8(b)), and therefore, to maintain the same value of C_PA, an increased energy extraction is expected. Figure 10(c) shows, in fact, increased induction factors.

Finally, the Trade-off configuration in Figure 10(d), which is also characterized by a reduced swept area (see Figure 8(c)), shows increased induction factors too. However, the chord lengths are larger than the maximum C_PA configuration to reduce the centrifugal stress, leading to a higher solidity than optimal.

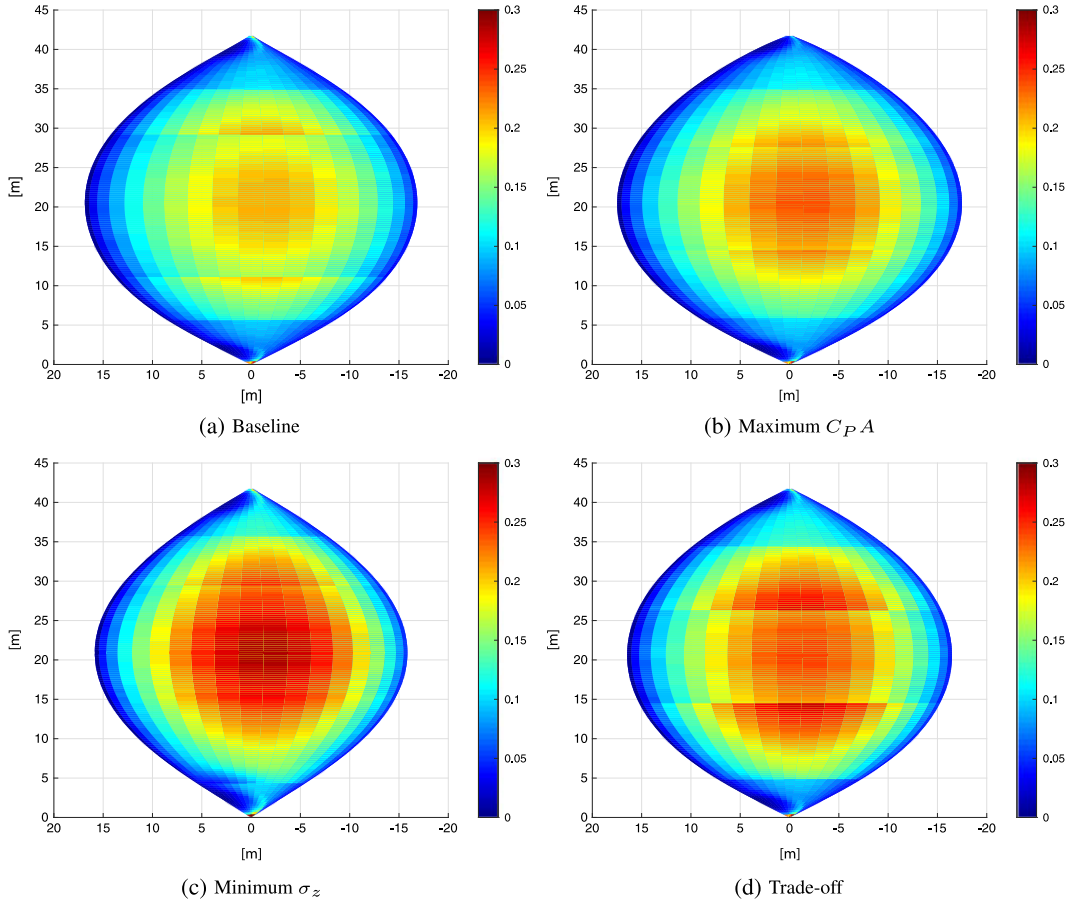

Figure 10. Contour plots of the upwind induction factor for the baseline and optimized configurations operating at the maximum power coefficient conditions. (a) Baseline, (b) Maximum $C_P A$, (c) Minimum σ_Z and (d) Trade-off.

3.2. Structural analysis

The maximum total values of the flatwise stress σ_z, useful to conduct the design process, for the Baseline and optimized configurations operating at the maximum power coefficient conditions, are reported in Figure 11.

The Minimum σ_z configuration is characterized by a smaller swept area, but chord values sensibly increased, especially in the top section, see Figure 8(b). All the three selected configurations show an increase in chord length in this segment. This provides a decrease in the flatwise stress in correspondence of the shaft link, where a peak is registered in the baseline configuration, as can be seen in Figure 11(a).

High stress values are also registered in the second, fourth and fifth segment from the top, where the baseline configuration provides a flatwise stress up to 60 MPa. The stress is mainly linked to the inertial contribution of the centrifugal force, whereas the aerodynamic forces provide only a limited contribution.[21,22] The Minimum σ_z configuration presents reduced peaks, see Figure 11(c), obtained both by decreasing the rotor maximum radius and increasing the airfoil section, leading to an increased mass but also an increased inertia. A partial reduction is registered for the Maximum $C_P A$ configuration, see Figure 11(b), which however presents a maximum peak up to 50 MPa.

The central segment in the Maximum $C_P A$ configuration presents a lower stress value than the Minimum σ_z configuration. The latter configuration is characterized, in fact, by an incremented chord length, with both aerodynamic performance and the centrifugal effects increased.

The Trade-off configuration presents a stress distribution similar to the Maximum $C_P A$ configuration, see Figure 11(d). Higher values are registered in the central and fourth segments from the top because of the larger radius with respect to the Minimum σ_z configuration and larger chord length with respect to the Maximum $C_P A$ configuration. Average stress is lower than in Baseline configuration, but stress peaks are comparable.

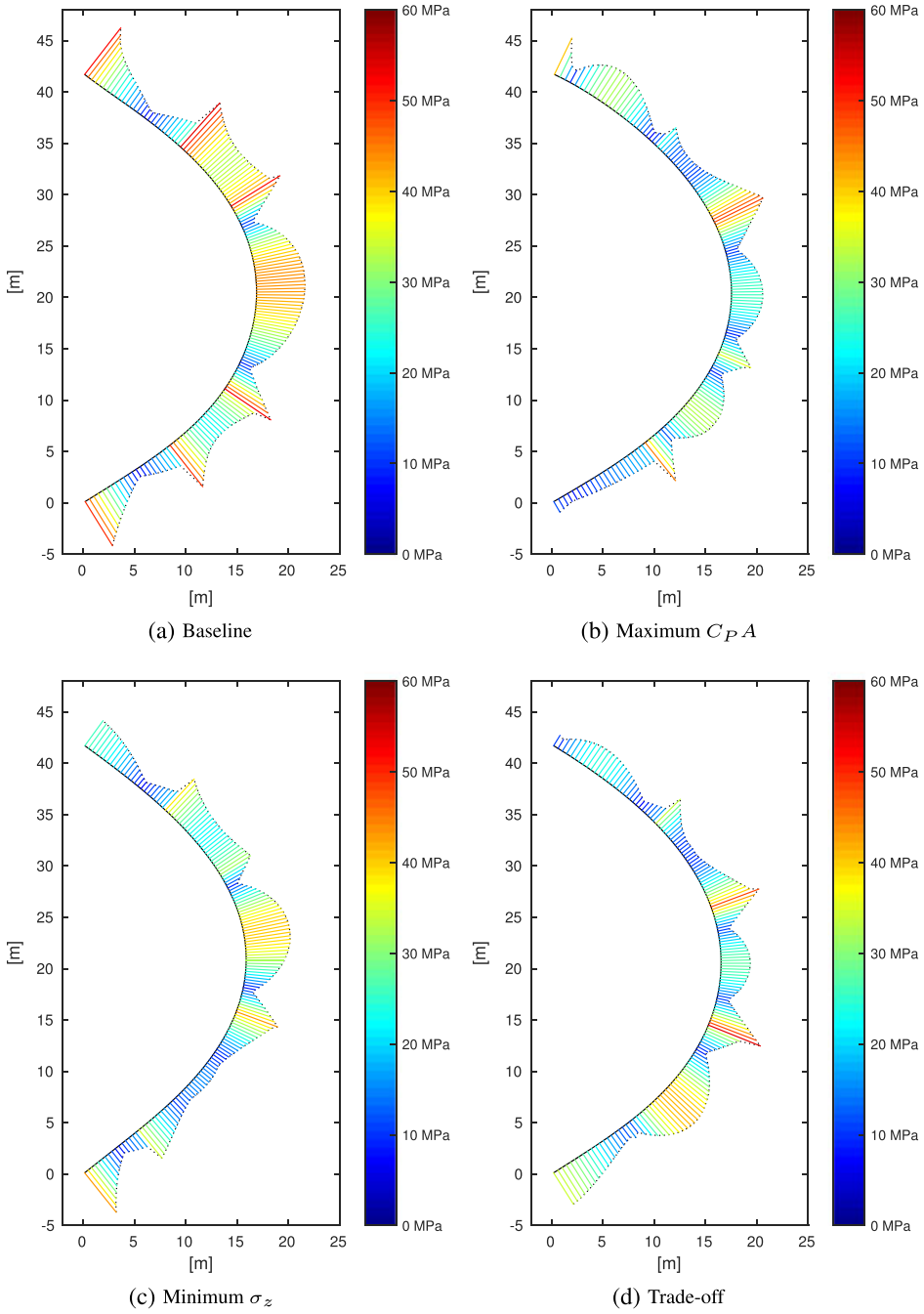

Figure 11. Contour plots of the flatwise stress along the blade length for the baseline and the different optimized configurations operating at the maximum power coefficient conditions. (a) Baseline, (b) Maximum C_PA, (c) Minimum σ_Z and (d) Trade-off.

The structural design needs, however, to be conducted also considering the mean stress and its cycle amplitude to perform fatigue analysis. Despite these, values are not considered as targets in the optimization process; their value can be estimated post-processing the results and are reported in Table IV.

Both the mean stress and the cycle amplitude are reduced in the Minimum σ_z configuration compared with the Baseline configuration, even though the mean stress is higher than in the Maximum C_PA and Trade-off configurations. Values are, however, sensibly reduced proving, therefore, that this optimization target scheme can also contribute to reduce the fatigue loads. Whether the fatigue design needs to be particularly considered in structural design, an additional optimization target can be considered.

Table IV. Mean, maximum and minimum stress and cycle amplitude for the baseline, and the different optimized configurations operating at the maximum power coefficient conditions.

Configuration	σ_Z,mean [MPa]	σ_Z,max [MPa]	σ_Z,min [MPa]	$\Delta\sigma_Z$z [MPa]
Baseline	32.2940	57.2574	8.0732	49.1841
Maximum C_PA	23.7568	52.5699	8.4595	44.1104
Minimum σ_Z	25.1233	49.1193	7.9687	41.1506
Trade-off	23.9713	54.3391	7.7365	46.6026

4. CONCLUSION

The aerodynamic model based on BEM theory and the structural model adopting Euler–Bernoulli beam elements were correctly validated for the Sandia 34 m Darrieus rotor, considered as Baseline configuration, against experimental data and surrogate models provided by commercial software. These models were coupled with an optimization algorithm based on the genetic theory, allowing to perform and evaluate variations of the blade shape and chord distribution.

The optimization routine, targeted to increase the aerodynamic performance and reduce the maximum blade stress of the Baseline rotor, provided a Pareto front populated with different configurations. A particular sector of this front, whose individuals dominate the Baseline configuration, is investigated from the aerodynamic and structural point of view.

From the aerodynamic analysis, an improvement in the rotor power production up to 8% is registered. The efficiency increase is obtained both with an increase of the swept area and a decrease in the tip speed ratio. On the other hand, the structural analysis showed a decrease in maximum stress up to 16%, obtained with a configuration that preserves the same aerodynamic production.

A Trade-off solution is also selected, which outperforms the Baseline configuration in both the targets. The analysis showed that, despite this, configuration can be obtained by small modifications from the Baseline design, it should be preferred since a significant increase in performance and reduction in stress is provided. The reduction in rotor investment cost and the increase in the energy production can possibly lead, in fact, to a lower cost of energy.

REFERENCES

1. Sutherland HJ, Berg DE, Ashwill TD. A Retrospective of VAWT Technology. *Technical Report*, Sandia National Laboratories Report SAND2012-0304, 2012.
2. Paulsen US, Pedersen TF, Madsen HA, Enevoldsen K, Nielsen PH, Hattel JH, Zanne L, Battisti L, Brighenti A, Lacaze M, Lim V, Heinen JW, Berthelsen PA, Carstensen S, De Ridder E-J, van Bussel GJW, Tescione G. Deepwind - an innovative wind turbine concept for offshore. *EWEA 2011 Conference*, Brussels, Belgium, 2011. [Online]. Available: http://proceedings.ewea.org/annual2011/allfiles2/1269_EWEA2011presentation.pdf (Accessed on October 2015).
3. [Online]. Available: http://www.inflow-fp7.eu/(Accessed on February 2015).
4. Paulsen US, Vita L, Madsen HA, Hattel JH, Ritchie E, Leban KM, Berthelsen PA, Carstensen S. 1st DeepWind 5 MW baseline design. *Energy Procedia* 2012; **24**: 27–35.
5. Berg DE. Structural design of the Sandia 34-meter vertical-aaxis wind Turbine. *Technical Report*, Sandia National Laboratories Report SAND84-1287, 1985.
6. Bedon G, De Betta S, Benini E. A computational assessment of the aerodynamic performance of a tilted Darrieus wind turbine. *Journal of Wind Engineering and Industrial Aerodynamics* 2015; **145**: 263–269. [Online]. Available: http://linkinghub.elsevier.com/retrieve/pii/S0167610515001683 (Accessed on October 2015).
7. Strickland JH. The Darrieus turbine: A performance prediction model using multiple streamtubes. *Technical Report*, Sandia National Laboratories Report SAND75-0431, 1975. [Online]. Available: http://scholar.google.com/scholar?hl=en&btnG=Search&q=intitle:The+Darrieus+Turbine:+A+performance+prediction+model+using+multiple+streamtubes% #2 (Accessed on October 2015).
8. Paraschivoiu I. Double-multiple streamtube model for Darrieus in turbines. *Wind turbine dynamics*, Nasa Conference Publication 2185, Cleveland, Ohio, USA, 1981; 19–25. [Online]. Available: http://onlinelibrary.wiley.com/doi/10.1002/cbdv.200490137/abstracthttp://adsabs.harvard.edu/abs/1981wtd..nasa...19P (Accessed on October 2015).
9. Paraschivoiu I, Delclaux F. Double multiple streamtube model with recent improvements. *Journal of Energy* 1983; **7**(3): 250–255. [Online]. Available: http://adsabs.harvard.edu/abs/1983JEner...7..250P (Accessed on October 2015).
10. Strickland JH, Webster BT, Nguyen T. A vortex model of the darrieus turbine: an analytical and experimental study. *Journal of Fluids Engineering* 1979; **101**(4): 500-505. [Online]. Available: http://www.csa.com/partners/viewrecord.php?requester=gs&collection=TRD&recid=A8018620AH (Accessed on October 2015).

11. Antonini EGA, Bedon G, De Betta S, Michelini L, Raciti Castelli M, Benini E. Innovative discrete vortex model for dynamic stall simulations. *American Institute of Aeronautics and Astronautics Journal* 2014; **53**(2): 479–485.
12. Madsen HA, Paulsen US, Vita L, Paulsen U. Vita L. Analysis of VAWT aerodynamics and design using the Actuator Cylinder flow model. *Journal of Physics: Conference Series* 2014; **555**(1): 012065. IOP Publishing (Accessed on October 2015).
13. Paraschivoiu I. *Wind Turbine Design: With Eemphasis on Darrieus Concept*. Polytechnic International Press: Montréal, Canada, 2002. [Online]. Available: http://books.google.com/books?hl=en&lr=&id=sefVtnVgso0C%&oi=fnd&pg=PR5&dq=Wind+turbine+design:+with+emphasis+on+Darrieus+concept&ots=Hkx_xSou2e&sig=s2tJhTcsEyUPaZ3hOvwNvF-csZc (Accessed on October 2015).
14. Masson C, Leclerc C, Paraschivoiu I. Appropriate dynamic-stall models for performance predictions of VAWTs with NLF blades. *International Journal of Rotating Machinery* 1998; **4**(2): 129–139. [Online]. Available: http://www.hindawi.com/journals/ijrm/1998/950151/abs/ (Accessed on October 2015).
15. Battisti L, Pinamonti P, Zanne L. Fluid Dynamic Modelling of Wind Turbines, 2010.
16. Shires A. Development and evaluation of an aerodynamic model for a novel vertical axis wind turbine concept. *Energies* 2013may; **6**(5): 2501–2520. [Online]. Available: http://www.mdpi.com/1996-1073/6/5/2501/ (Accessed on October 2015).
17. Ashwill TD. Initial structural response measurements and model validation for the Sandia 34-meter VAWT test bed. *Technical Report*, Sandia National Laboratories Report SAND88-0633, 1990.
18. Akin D. Response of an off shore wind turbine to simultaneous wind and wave loads, *M.Sc. Thesis- Danmarks Tekniske Universitet*, 2011.
19. Larsen TJ, Madsen HA. On the way to reliable aeroelastic load simulation on VAWT's. *Ewea 2013 Conference*, Wien, Austria, 2013. [Online]. Available: http://forskningsbasen.deff.dk/Share.external?sp=Sc2cdd4e3-3cfc-464b-952e-180d875d8634&sp=Sdtu (Accessed on October 2015).
20. Hansen MOL, Sørensen JN, Voutsinas SG, Sørensen NN, Madsen HA. State of the art in wind turbine aerodynamics and aeroelasticity. *Progress in Aerospace Sciences* 2006; **42**(4): 285–330. [Online]. Available: http://linkinghub.elsevier.com/retrieve/pii/S0376042106000649 (Accessed on October 2015).
21. Raciti Castelli M, Dal Monte A, Quaresimin M, Benini E. Numerical evaluation of aerodynamic and inertial contributions to Darrieus wind turbine blade deformation. *Renewable Energy* 2013; **51**: 101–112. [Online]. Available: http://dx.doi.org/10.1016/j.renene.2012.07.025http://www.sciencedirect.com/science/article/pii/S096014811200451X (Accessed on October 2015).
22. Raciti Castelli M, De Betta S, Benini E. Numerical evaluation of the contribution of inertial and aerodynamic forces on VAWT blade loading. *World Academy of Science, Engineering and Technology* 2013; **78**: 373–378. [Online]. Available: http://www.researchgate.net/publication/236869265_Numerical_Evaluation_of_the_Contribution_of_Inertial_and_Aerodynamic_Forces_on_VAWT_Blade_Loading/file/9c9605220903d3d62e.pdf (Accessed on October 2015).
23. Blackwell BF, Reis GE. Blade shape for a troposkien type of vertical-axis wind turbine. *Technical Report*, Sandia National Laboratory SLA-74-0154, Albuquerque, New Mexico, 1977. [Online]. Available: http://www.osti.gov/energycitations/product.biblio.jsp?osti_id=7257563 (Accessed on October 2015).
24. Reis GE, Blackwell BF. Practical approximations to a troposkien by straight-line and circular-arc segments. *Technical Report*, Sandia National Laboratories Report SAND74-0100, 1975. [Online]. Available: http://www.osti.gov/energycitations/product.biblio.jsp?osti_id=5115217 (Accessed on October 2015).
25. Ashwill TD. Measured data for the Sandia 34-meter vertical axis wind turbine. *Technical Report*, Sandia National Laboratories Report SAND91-2228, 1992. [Online]. Available: http://infoserve.sandia.gov/sand_doc/1991/912228.pdf (Accessed on October 2015).
26. Paulsen US, Madsen HA, Hattel JH, Baran I, Hørlyck Nielsen P. Design optimization of a 5 MW floating offshore vertical-axis wind turbine. *Energy Procedia* 2013; **35**: 22–32. [Online]. Available: http://www.sciencedirect.com/science/article/pii/S1876610213012411 (Accessed on October 2015).
27. Roscher B, Ferreira CS, Bernhammer LO, Madsen HA, Griffith DT, Stoevesandt B. Combined structural optimization and aeroelastic analysis of a Vertical Axis Wind Turbine. *AIAA SciTech - 33rd Wind Energy Symposium*, Kissimmee, Florida, USA, 2015; 1–11. (Accessed on October 2015).
28. Deb K. Multi-objective optimization using evolutionary algorithms. In *Multi-objective optimization*. John Wiley & Sons: Hoboken, NJ, 2001; 13–46. [Online]. Available: http://scholar.google.com/scholar?hl=en&btnG=Search&q=intitle:Multi-Objective+Optimization+Using+Evolutionary+Algorithms#0 (Accessed on October 2015).

29. Glauert H. Airplane propellers. In *Aerodynamic Theory*. Springer Berlin Heidelberg,Heidelberg, Germany, 1935; 169–360. [Online]. Available: http://scholar.google.com/scholar?hl=en&btnG=Search&q=intitle:Airplane+Propellers#0 (Accessed on October 2015).
30. Bedon G, Antonini EGA, De Betta S, Raciti Castelli M, Benini E. Evaluation of the different aerodynamic databases for vertical axis wind turbine simulations. *Renewable & Sustainable Energy Reviews* 2014; **40**: 386–399.
31. Jacobs EN. The aerodynamic characteristics of eight very thick airfoils from tests in the variable density wind tunnel. *Technical Report*, National Advisory Committee for Aeronautics 391, 1932. [Online]. Available: http://naca.central.cranfield.ac.uk/reports/1932/naca-report-391.pdf (Accessed on October 2015).
32. Gregorek GM, Hoffman MJ, Berchak MJ. Steady State and Oscillatory Aerodynamic Characteristics of a Sandia 0018/50 Airfoil. *Technical Report*, Aeronautical and Astronautical Research Laboratory, The Ohio State University, 1989.
33. Ansys Inc. *ANSYS Parametric Design Language 14.5 Guide*. ANSYS, Inc.: Canonsburg, PA, U.S.A. 2012.
34. Timoshenko S. *History of Strength of Materials*, 1983. [Online]. Available: http://books.google.co.in/books/about/History_of_Strength_of%_Materials.html?id=tkScQmyhsb8C&pgis=1 (Accessed on October 2015).
35. Goldberg DE. *Genetic Algorithms in Search, Optimization, and Machine Learning*. Addison–Wesley Longman Publishing Co., Inc: Boston, Massachusetts, USA, 1989.
36. Matlab. [Online]. Available: Phttp://www.mathworks.com/help/gads/gamultiobj.html. (Accessed February 2015).